

Electronic Supplementary Information for

**Achieving long-term stable perovskite solar cells
via ion neutralization**

Hyungcheol Back^{a‡}, Geunjin Kim^{a‡}, Junghwan Kim^a, Jaemin Kong^a, Tae Kyun Kim^a,
Hongkyu Kang^a, Heejoo Kim^a, Jinho Lee^b, Seongyu Lee^b, Kwanghee Lee^{a,b*}

*^aHeeger Center for Advanced Materials & Research Institute for Solar and Sustainable
Energies, ^bSchool of Materials Science and Engineering, Gwangju Institute of Science and
Technology, Gwangju 61005, Republic of Korea*

*To whom correspondence should be addressed: klee@gist.ac.kr (K. Lee)

‡H. Back and G. Kim contributed equally to this work.

Methods

Materials

Lead (II) iodide (PbI_2) and Lead (II) bromide (PbBr_2) were purchased from Sigma Aldrich. Poly(3,4-ethylenedioxythiophene)-poly(styrenesulfonate) (PEDOT:PSS) (AI 4083) and phenyl- C_{60} -butyric acid methyl ester (PC_{60}BM) were purchased from Clevios and Nano-C, respectively. Methylammonium iodide ($\text{CH}_3\text{NH}_3\text{I}$) was prepared according to a previously published method¹. The 1.5M of perovskite solution was prepared by mixing the 1.35 mmol of PbI_2 , 0.15 mmol of PbBr_2 and 1.8 mmol of MAI powder in gamma butyrolactone and dimethyl sulfoxide mixed solution (7:3 v/v) at 60 °C for overnight.

Titanium (IV) isopropoxide (TTIP), niobium (V) ethoxide (NET), diethanolamine (DEA) and isopropyl alcohol (IPA) were purchased from Sigma Aldrich and used without re-distillation. For preparing pristine titanium suboxide (TiO_x) solution, TTIP was diluted by IPA with volume ratio of 1:300. For preparing amine-mediated titanium suboxide (AM- TiO_x) solution, TTIP (1 mol) was mixed with DEA (2 mol) and the precursor was diluted by IPA with volume ratio of 1:300. For preparing amine-mediated niobium suboxide (AM- NbO_x) solution, NET (1 mol) was mixed with DEA (2 mol) and the precursor solution was diluted by IPA with volume ratio of 1:300. Overall processes were conducted under nitrogen gas to prevent hydrolysis.

Vanadium (V) oxytriisopropoxide was purchased from Sigma Aldrich. For preparing vanadium suboxide (VO_x) solution, the precursor was diluted by IPA with volume ratio of 1:300.

Device Fabrication

For the fabrication of the p-i-n planar heterojunction (PHJ) type perovskite solar cells (PSCs), a solution of PEDOT:PSS (a 300- μl solution filtered through a 0.45 μm pore size

acetate filter) was first spin-cast onto a pre-cleaned indium-tin oxide (ITO) glass substrates at 5000 rpm for 40 s and then dried at 150 °C for 10 min under ambient conditions. The VO_x solution (70 μl) was then spin coated on PEDOT:PSS/ITO substrate at 3000 rpm for 30 s and was dried at same condition for 5 min. For the depositing the perovskite layers in N₂ filled globe box, the precursor solution (25 μl) was coated onto the VO_x/PEDOT:PSS/ITO substrate by a sequential two-step spin- cast process at 1000 and 4000 rpm for 30 and 60 s, respectively. After 25 s at the second spin-cast process, the perovskite layer was treated with toluene (800 μl) drop-casting then dried at 100 °C for 10 min. Afterward, a solution (a 30-μl solution filtered through a 0.45 μm PTFE filter) containing 4 wt.% PC₆₀BM in chlorobenzene was spin-cast at 1500 rpm for 40 s then AM-TiO_x was spin-coated at 5000 rpm for 30 s with a precursor solution of 60 μl and dried at 100 °C for 5 min as a the chemical inhibition layer (CIL). Finally, the p-i-n PHJ devices were completed by evaporating aluminum (Al), silver (Ag), or gold (Au) electrode (thickness of 150 nm) with 1 Å s⁻¹ rate through a shadow mask (area of 4.64, 25 36, and 64 mm²) under high vacuum (10⁻⁶ mbar); for X-ray photoelectron spectroscopy (XPS) measurements, all procedures for the XPS samples were the same as for the PSCs except the thickness of Ag electrodes with 5 nm.

For the fabrication of the electron-only devices, a C₆₀ layer (40 nm) was vacuum deposited onto an ITO glass substrates with 0.2 Å s⁻¹ rate under high vacuum (10⁻⁶ mbar). For the depositing the perovskite layers (300 nm) in N₂ filled globe box, the precursor solution (25μl) was coated onto the C₆₀/ITO substrate by a sequential two-step spin-cast process at 1000 and 5000 rpm for 30 and 60 s, respectively. After 25 s at the second spin-cast process, the perovskite layer was treated with diethyl ether (400 μl) drop-casting then dried at 100 °C for 10 min. Afterward, a solution containing 4 wt.% PC₆₀BM in chlorobenzene (a 30-μl solution filtered through a 0.45 μm PTFE filter) was spin-cast at 1500 rpm for 40 s then a solution of CIL (with a precursor solution of 60 μl) was spin-coated at 5000 rpm for 30 s and

dried at 100 °C for 5 min. Finally, the electron-only devices were completed by evaporating Al electrodes (thickness of 150 nm) with 1 Å s⁻¹ rate through a shadow mask (area of 4.64 mm²) under high vacuum (10⁻⁶ mbar).

For the fabrication of the Al (for an electrical resistance test) or ITO (for capacitance-voltage characteristics)/ TiO_x layer or CIL (60 nm)/Al devices, TiO_x (the precursor diluted by IPA with volume ratio of 1:100) were spin coated at 3000 rpm for 30 s on the pre-deposited Al (15 nm) or ITO substrate. Finally, the electron-only devices were completed by evaporating Al electrodes (thickness of 100 nm) with 1 Å s⁻¹ rate through a shadow mask (area of 4.64 mm²) under high vacuum (10⁻⁶ mbar).

Characterization

The current density-voltage (*J-V*) characteristics of the unit cells were measured (with a 100 ms delay) using a Keithley 238 source measure unit (Keithley Instruments, Inc., Cleveland, OH, USA) under air mass 1.5 global (AM 1.5G) simulated solar illumination emitted at 100 mW cm⁻² from a Newport 750 solar simulator without UV filter. Max power point (MPP) tracking of the devices were conducted under N₂ condition with a custom-built LabView program (National Instruments, Austin, TX), based on the perturb and observe (P&O) method (logic diagram represented in Figure S17).

Incident-photon-to-current-efficiency (IPCE) measurements of the PHJ perovskite solar cells were performed using a Solar Cell Spectral Response/QE/IPCE measuring system (PV Measurements, Inc., Boulder, CO, USA) with a chopping frequency of 100 Hz. The measuring systems were calibrated with an amorphous standard cell manufactured by (PV Measurements, Inc., Boulder, CO, USA).

Ultraviolet photoelectron spectroscopy (UPS) of the sample layer was obtained using He (I) (21.2 eV) source and a gold (Au) calibration at the Korea Basic Science Institute (KBSI,

Korea). UV-Vis spectra of the TiO_x and CIL on a fused silica substrate were characterized by a UV/Vis/NIR spectrometer (Lambda 750, Perkin Elmer, USA). The contact potential difference (CPD) measurements of the TiO_x and CIL on the ITO substrate were performed using Kelvin probe technique (KP6500, McAllister Technical Services). Capacitance-voltage (C-V) characteristics were measured with an Agilent 4284A LCR meter with a frequency of 10⁵ Hz and amplitude of 50 mV in the ITO/TiO_x or CIL (60 nm)/Al structure. Atomic force microscopy (AFM) images were obtained using an XE-100 (Park System, Korea) in non-contact mode. Scanning electron microscopy (SEM) top images of the samples were taken by a Hitachi S-4700 instrument. The thicknesses of the devices were measured using a surfcoorder (Kosaka Laboratory). Auger electron spectroscopy (AES) of the sample (ITO/PEDOT:PSS/VO_x/perovskite/PC₆₀BM/TiO_x or CIL) was taken using a PHI 710 Scanning Auger Nanoprobe instrument. The XPS measurements were performed in a VG Multilab 2000 (by using Al K α x-ray source) under high vacuum (10⁻⁹ mbar). The XPS spectra were calibrated by the binding energy of 285 eV for C 1s. Cross-section images of Scanning Electron Microscopy (SEM) were captured with a Hitachi S-4700 instrument. The impedance spectroscopy measurements of the PSCs with and without a CIL (active area of 4.64 mm²) were performed using a galvanostat mode (PGSTAT30, AutoLab, EcoChemie) at open-circuit condition, a voltage of 1.07 V in a frequency range between 0.1 and 1 MHz, under AM 1.5G simulated solar illumination emitted at 100 mW cm⁻² from a Newport 750 solar simulator. Transient photocurrent (TPC) measurements were performed by shorting the PSCs, ITO/PEDOT:PSS/VO_x/Perovskite/PC₆₀BM/with or without CIL/Ag across a resistor. A 6 ns optical pulse from a 532 nm (with an intensity \sim 10 μ J cm⁻²) using the frequency-doubled outputs of a Nd:YAG laser (LOTIS) was applied. The resulting current transient was measured using an oscilloscope (TDS520/Tektronix).

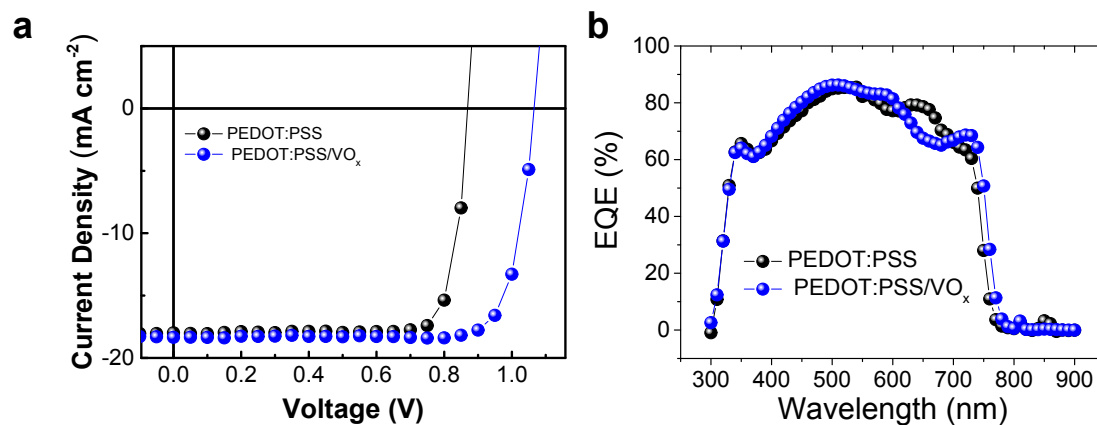


Figure S1. a,b, J - V characteristics and IPCE spectra of p-i-n PHJ perovskite solar cells with and without the VO_x layers.

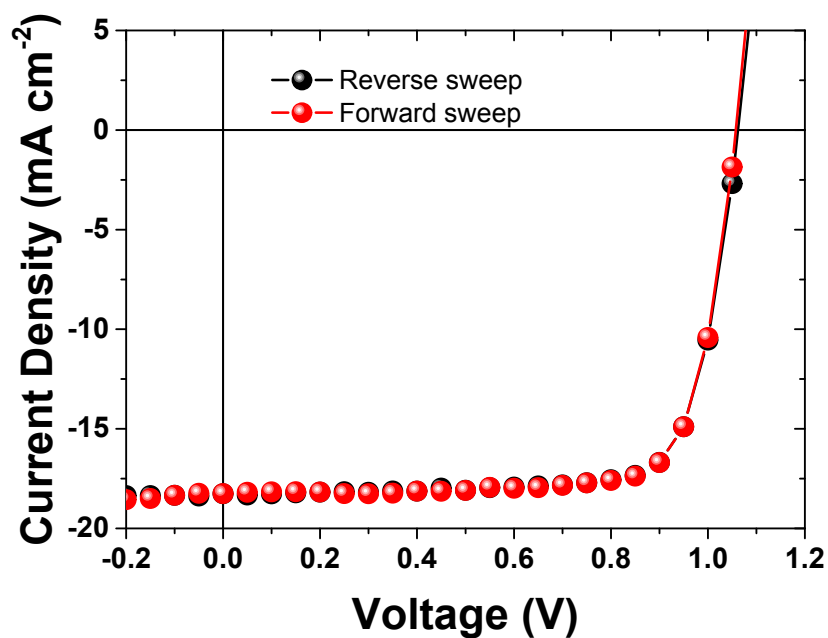


Figure S2. J - V characteristics of p-i-n PHJ perovskite solar cells measured by forward and reverse scans.

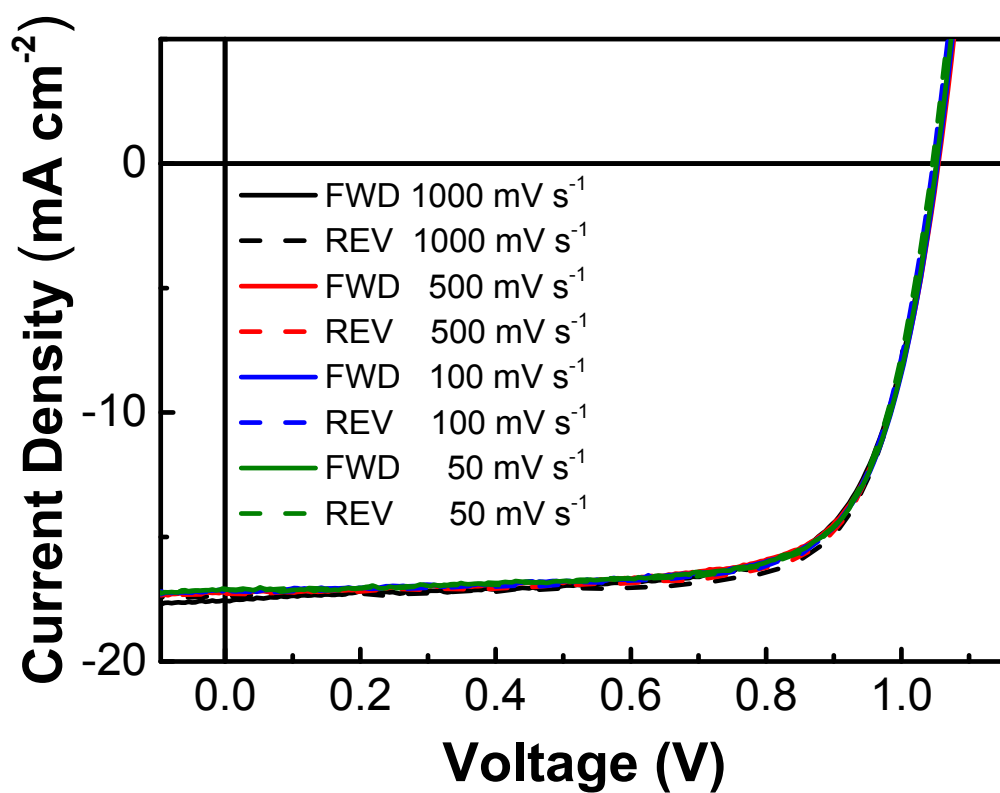


Figure S3. Scan rate test in J - V characteristics. Forward and reverse scan of the J - V curve of the device with CIL as a function of scan rate (mV s^{-1}).

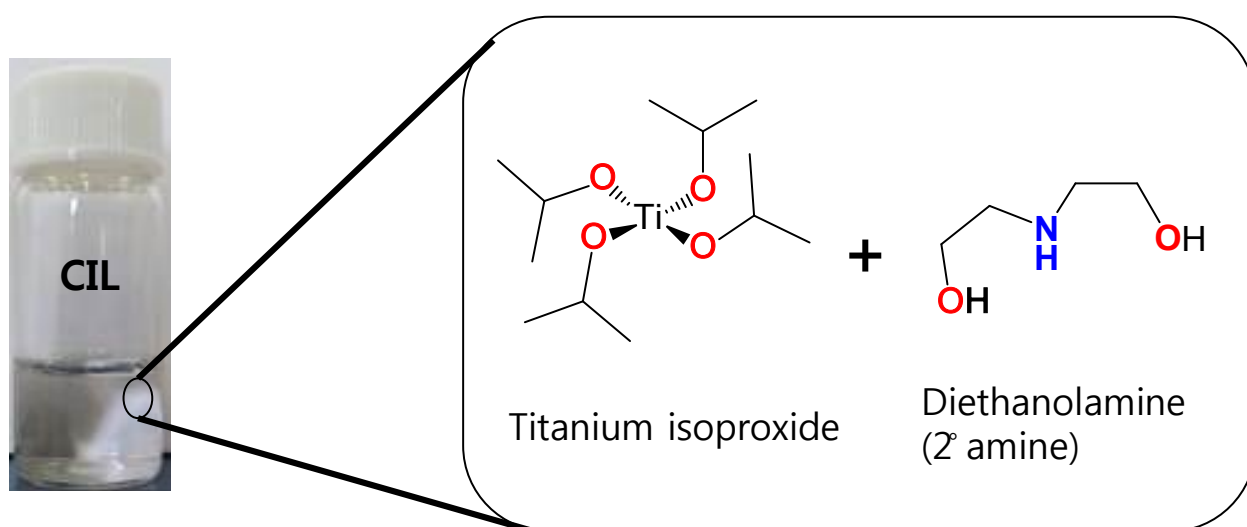


Figure S4. Image of the solution and chemical components of the CIL.

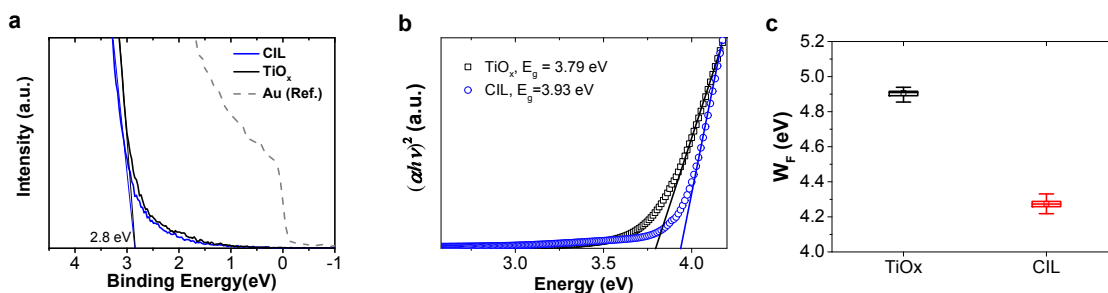


Figure S5. (a) UPS and (b) UV-Vis spectra of the TiO_x and CIL. (c) Workfunction (WF) of TiO_x and CIL measured by Kelvin probe.

Note S1. We obtained their highest occupied molecular orbital (HOMO) energy levels of -8.0 eV with respect to the Fermi level of the gold reference (5.2 eV) as shown in the Figure S5a from the onset binding energy (2.8 eV) of the ultraviolet photoelectron spectroscopy (UPS) of the titanium suboxide layer (TiO_x) and AM- TiO_x layer (CIL). The lowest unoccupied energy molecular orbital (LUMO) energy levels of the TiO_x (-4.21 eV) and CIL (-4.07 eV) were also deduced from the energy gaps (3.79 eV for TiO_x and 3.93 eV for CIL) using the UV-Vis spectra of the layers as shown in Figure S5b. Furthermore, we measured the effective workfunctions (WFs) of the TiO_x and CIL on the ITO substrate (4.90 ± 0.02 eV for TiO_x and 4.27 ± 0.03 eV for CIL) using the Kelvin probe method (Figure S5c).

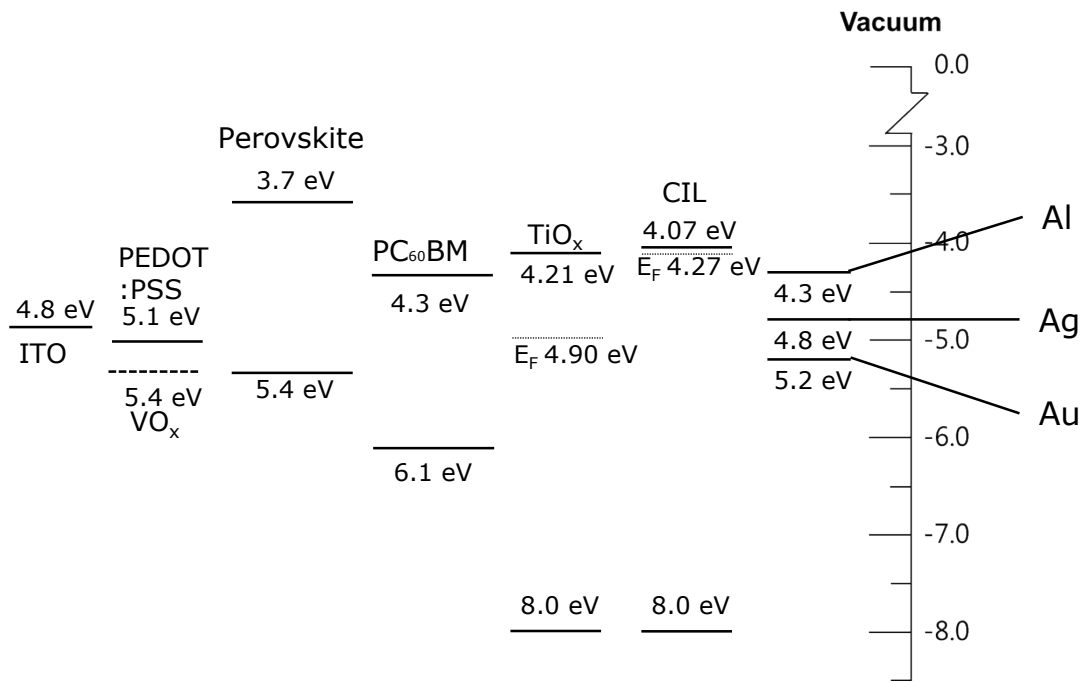


Figure S6. Energy levels of the p-i-n PHJ perovskite solar cells applied by the TiO_x and CIL.

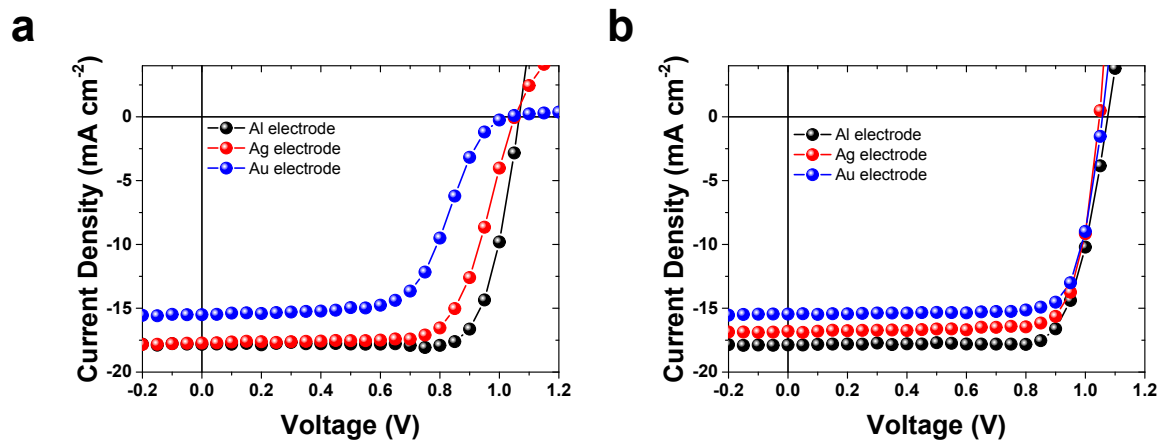


Figure S7. a,b, J - V curves of p-i-n PHJ devices using different cathodes, such as Al, Ag, Au, and without and with a CIL.

Note S2. Because the solution process to create a pin-hole-free PC₆₀BM layer on the rough high-crystalline perovskite surface is difficult, the direct contact between the perovskite layer and the top metal electrode often causes electrical problems, such as an electrical barrier blocking electron extraction. When the high-WF metal electrodes, such as Ag (4.8 eV) or Au (5.2 eV), are applied to the reference device structure, direct contact between the metal electrode and perovskite layer impedes electron extraction and often causes a high R_s in the J - V characteristics of the devices (Figures S6 and S7).

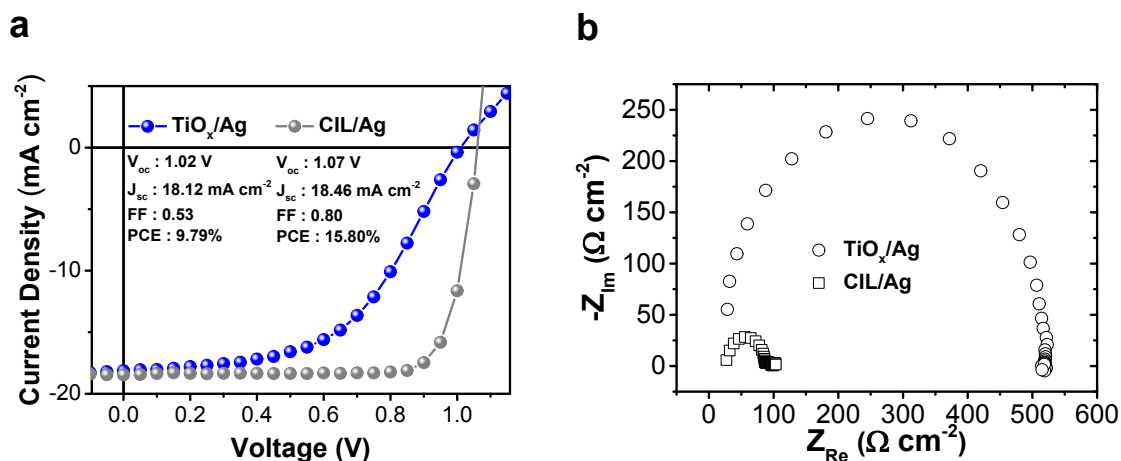


Figure S8. a,b, J - V characteristics and impedance of PSCs with TiO_x and CIL measured under the illumination of AM 1.5G.

Note S3. The TiO_x and CIL exhibit different device performance as shown in the Figures S8a; whereas the device with CIL represents high fill factor (FF) of 80%, the device with TiO_x shows low FF of 53%. This performance can be interpreted as a result of the different electrical properties between TiO_x and CIL as shown in Figures S5-S7. The relatively high WF (4.90 eV) of the TiO_x is not suitable to the electron extraction from the PC₆₀BM to Ag cathode due to mismatched energy levels, as shown in Figures S5 and S6, whereas the CIL

exhibits sufficiently low WF (4.27 eV) enough to extract from the PC₆₀BM to Ag. In addition to the undesirable energy levels of the TiO_x, its low electrical resistance also increases the series resistance of the devices, as shown in a large impedance loop (Figure S8b).

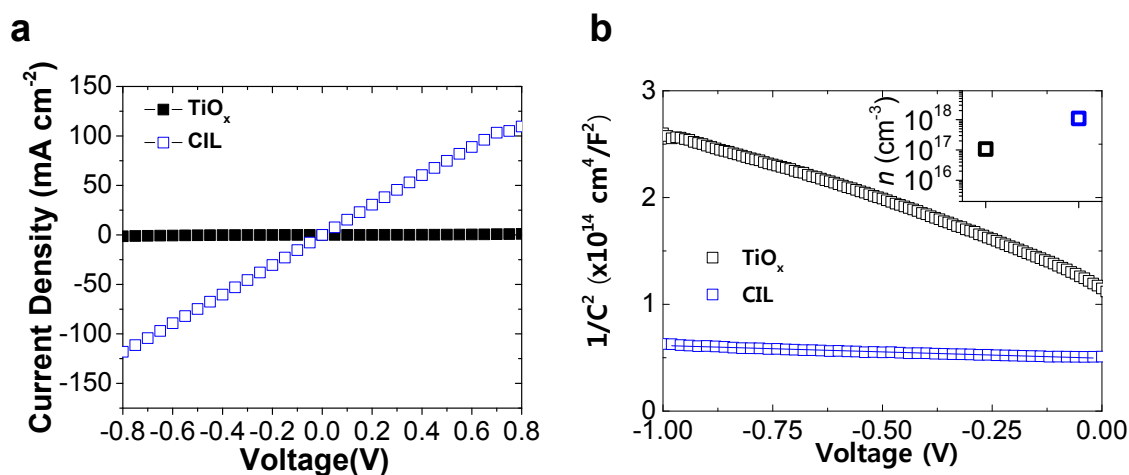


Figure S9. a,b, J - V characteristics and C^{-2} - V characteristic of TiO_x and CIL. The inset represents carrier density of both layers.

Note S4. We measured J - V characteristics of Al/TiO_x or CIL (60 nm)/Al devices and the CIL exhibits much lower electrical resistance than that of TiO_x as shown in the Figure S9a, whose reduced resistance and WF (in Figure S5c and S6) implies that CIL is a doped semiconductor. To directly measure the carrier density of the doped CIL, we conducted a capacitance-voltage (C-V) measurement on the TiO_x and CIL with a frequency of 10⁵ Hz and amplitude of 50 mV in the ITO/TiO_x or CIL (60 nm)/Al structure. A higher carrier density ($\sim 10^{18}$ cm⁻³) of the CIL than that of the TiO_x ($\sim 10^{17}$ cm⁻³) clearly represents the properties of a doped semiconductor (Figure S9b). The charge carrier densities (N_{DS}) of the TiO_x and CIL are obtained from the general theory of the Schottky contact as follows²,

$$N_D = \frac{2}{q\epsilon_0\epsilon_r} \left[-\frac{1}{d(C^{-2})/dV} \right] \quad (\text{S1})$$

Equation (S1), where $q = 1.69 \times 10^{-19}$ C is the elementary charge, $\epsilon_0 = 8.85 \times 10^{-14}$ F cm⁻¹ is the permittivity in vacuum and $\epsilon_r = 9$ is the relative permittivity of TiO_x and CIL³.

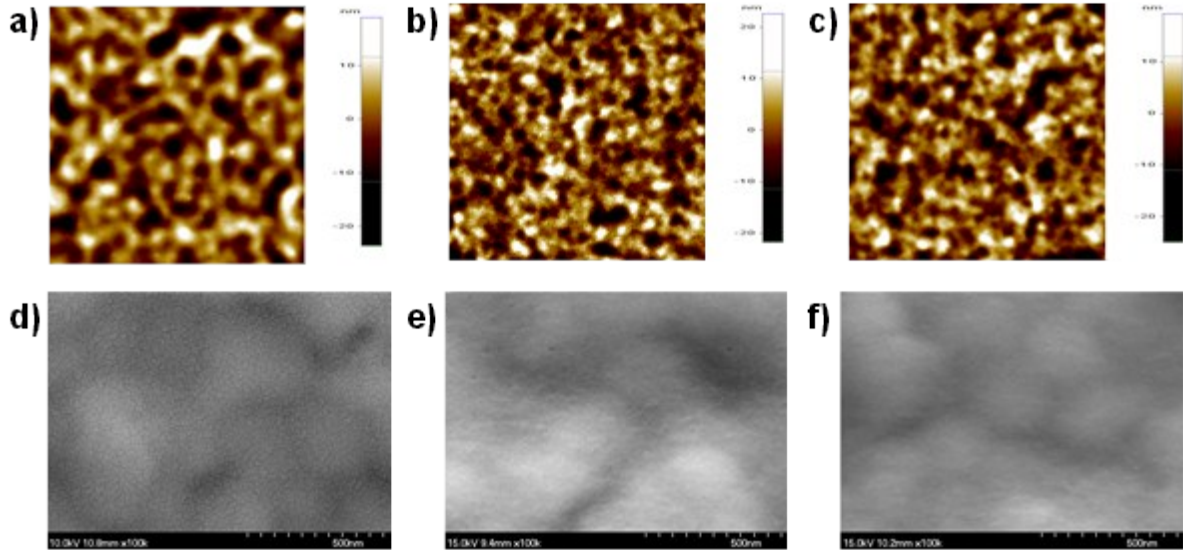


Figure S10. Atomic force microscopy (AFM) and SEM images of a, d PC₆₀BM, b, e TiO_x on a PC₆₀BM layer and c, f CIL on a PC₆₀BM layer. The scale in the AFM images is 10 μm × 10 μm area and the root-mean-square roughness (RMS) values of the layers are 5.90, 5.80, and 5.59 nm, respectively. The scale bars in the AFM and SEM images represent 1 μm and 500 nm, respectively.

Note S5. We conducted atomic force microscopy (AFM) and scanning electron microscopy (SEM) studies to check the morphology of the samples with the structures of ITO/PEDOT:PSS/VO_x/perovskite/PC₆₀BM and ITO/PEDOT:PSS/VO_x/perovskite/PC₆₀BM/TiO_x or CIL. Based on the AFM data and SEM images (Figures S10d), the PC₆₀BM layer (RMS ~ 5.90 nm) on the perovskite layer shows the small grain. Interestingly, after deposition of the TiO_x and CIL on PC₆₀BM layers, its surface morphology exhibited more smooth (RMS ~ 5.80 nm and 5.59 nm, respectively) surface and its grain boundary was disappeared.

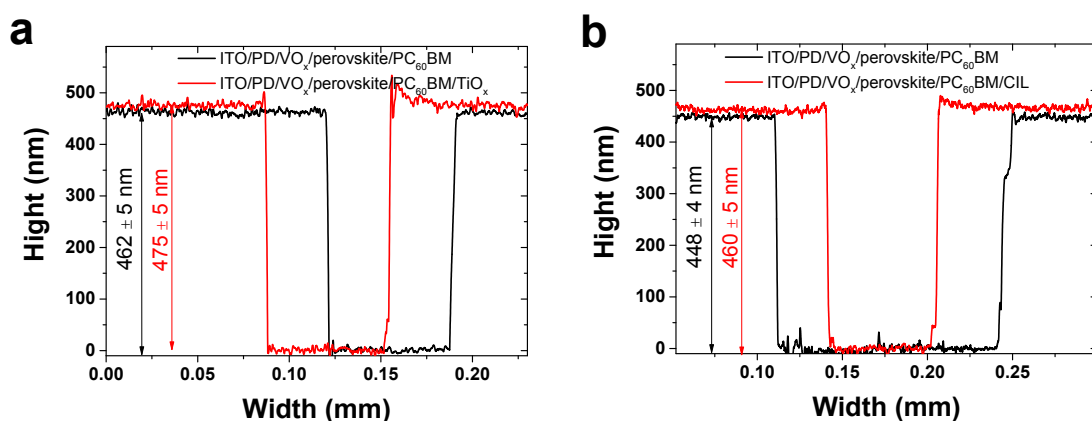


Figure S11. The thickness profiles of the devices (ITO/PEDOT:PSS/VO_x/perovskite/PC₆₀BM) before and after depositing the TiO_x (~ 13 nm) and CIL (CIL, ~ 12 nm) layers.

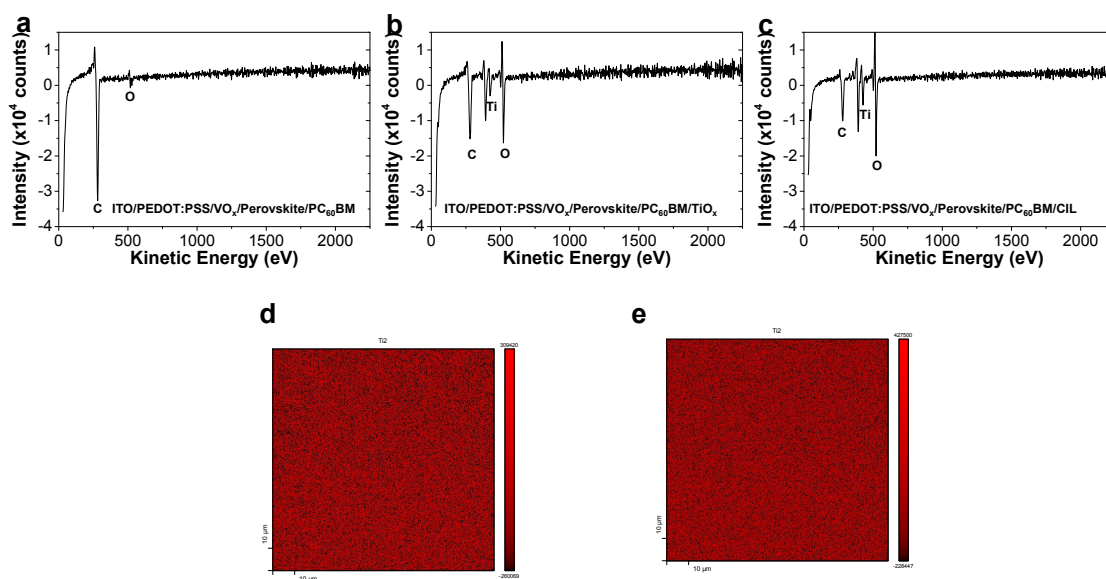


Figure S12. a, b, c, the auger electron spectroscopy of PC₆₀BM on the perovskite layer, TiO_x on PC₆₀BM layer and CIL on PC₆₀BM layer. d,e image mapping of titanium on TiO_x and CIL on PC₆₀BM layers.

Note S6. We measured the auger electron spectroscopy (AES) of the TiO_x/CIL and conducted the AES mapping of titanium atoms in the layers. As shown in Figure S12, the TiO_x and CIL were uniformly deposited on PC_{60}BM layer. Based on the results, we believe that the TiO_x and CIL fully cover the PC_{60}BM .

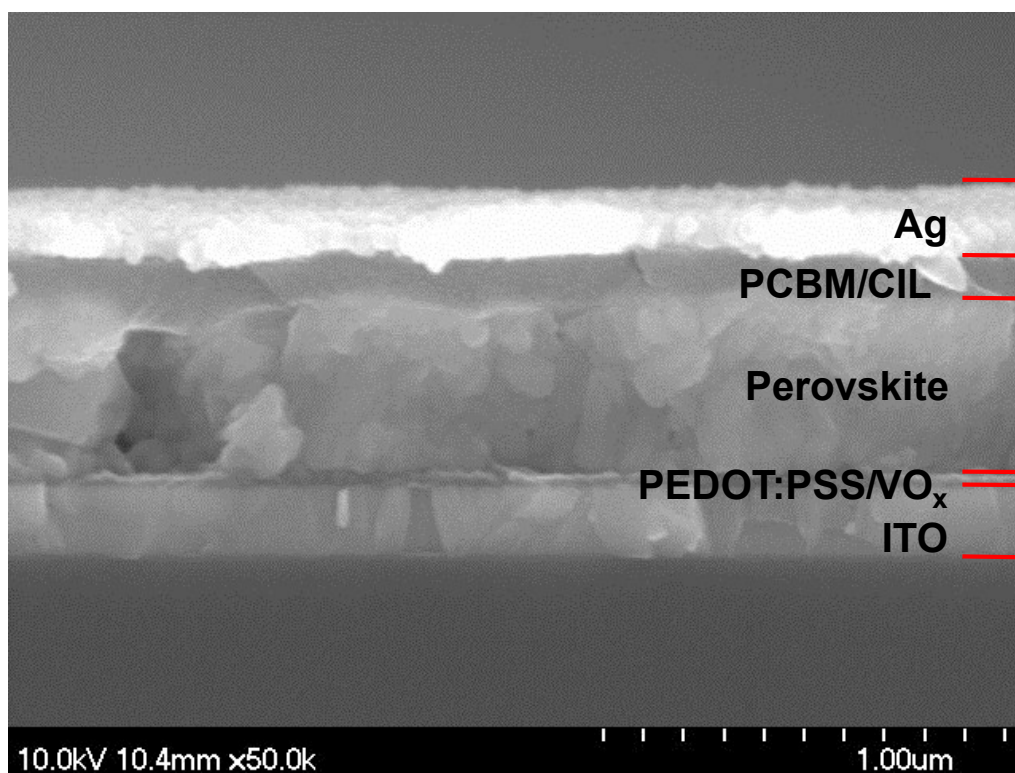


Figure S13. Cross sectional SEM image of a CIL device.

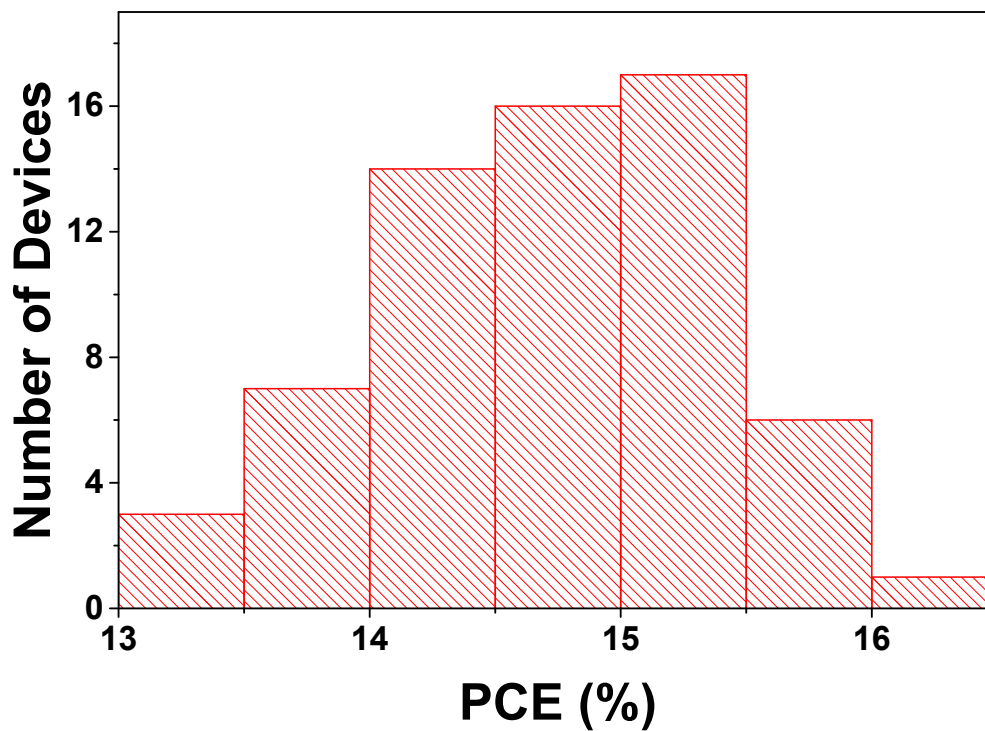


Figure S14. Histogram of the average efficiencies for 64 PSCs.

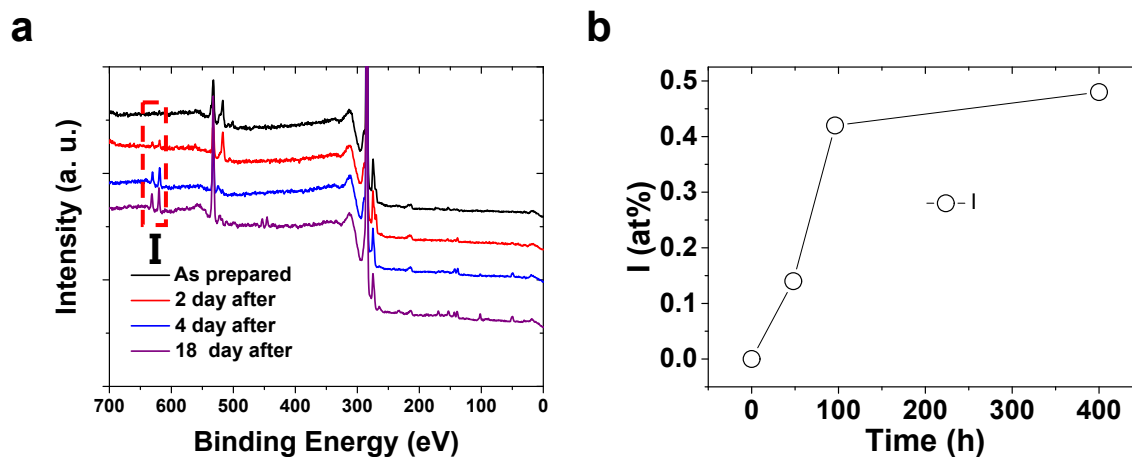


Figure S15. a,b, Overview of XPS spectra and atomic percentages of the iodine component of the PC₆₀BM/perovskite/VO_x/PEDOT:PSS/ITO corresponding to ageing time.

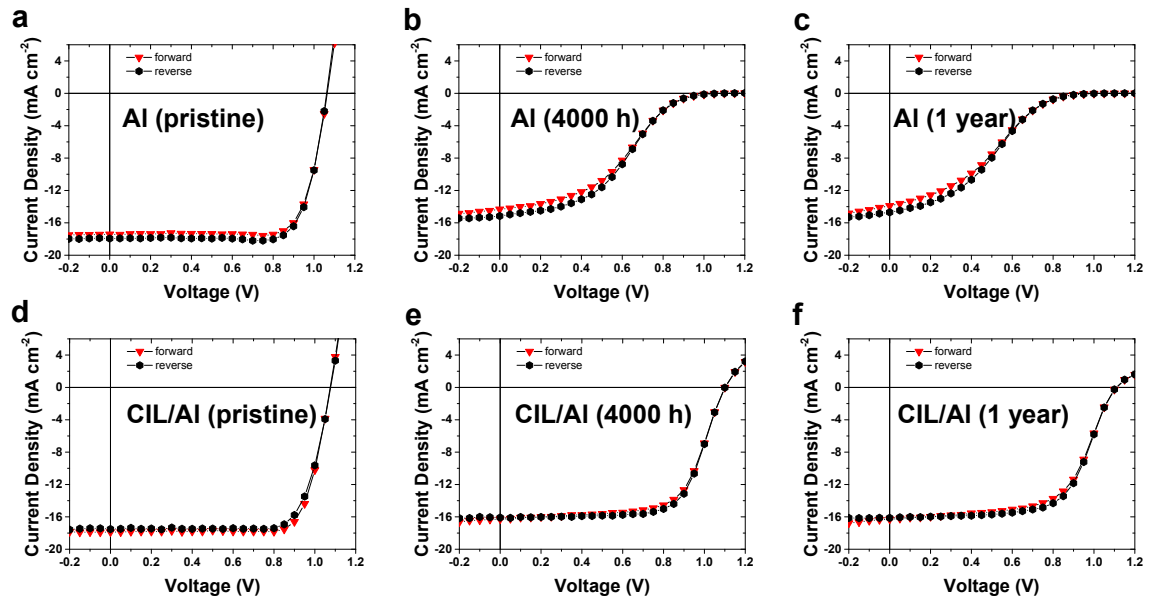


Figure S16. J - V characteristics of pristine, 4000 h-aged and 1-year aged devices. Forward and reverse scan of the J - V curve of the device without and with CIL as a function of time (h).

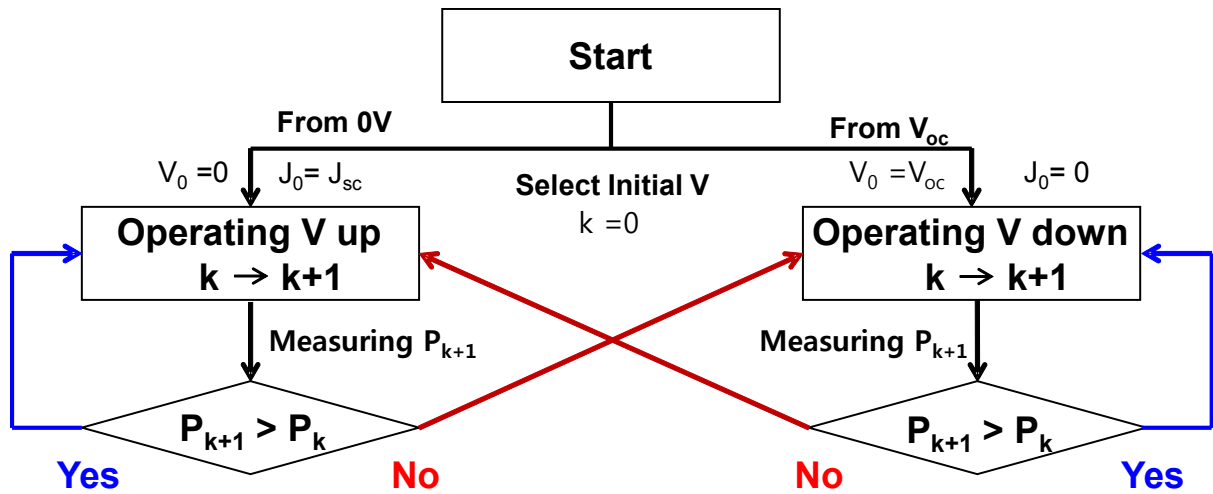


Figure S17. Logic diagram of a perturb and observe (P&O) method for max power point (MPP) tracking of the devices.

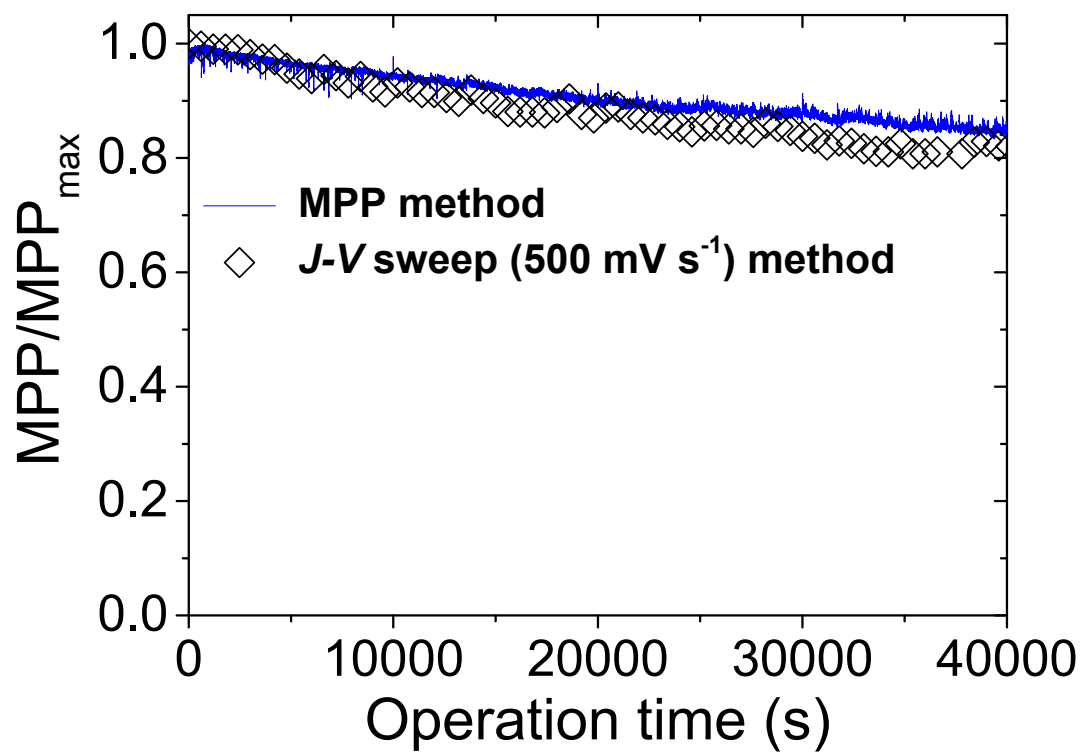


Figure S18. The J - V sweep and the steady-state photocurrent measurements (MPP tracking) of CIL devices under AM 1.5 illumination.

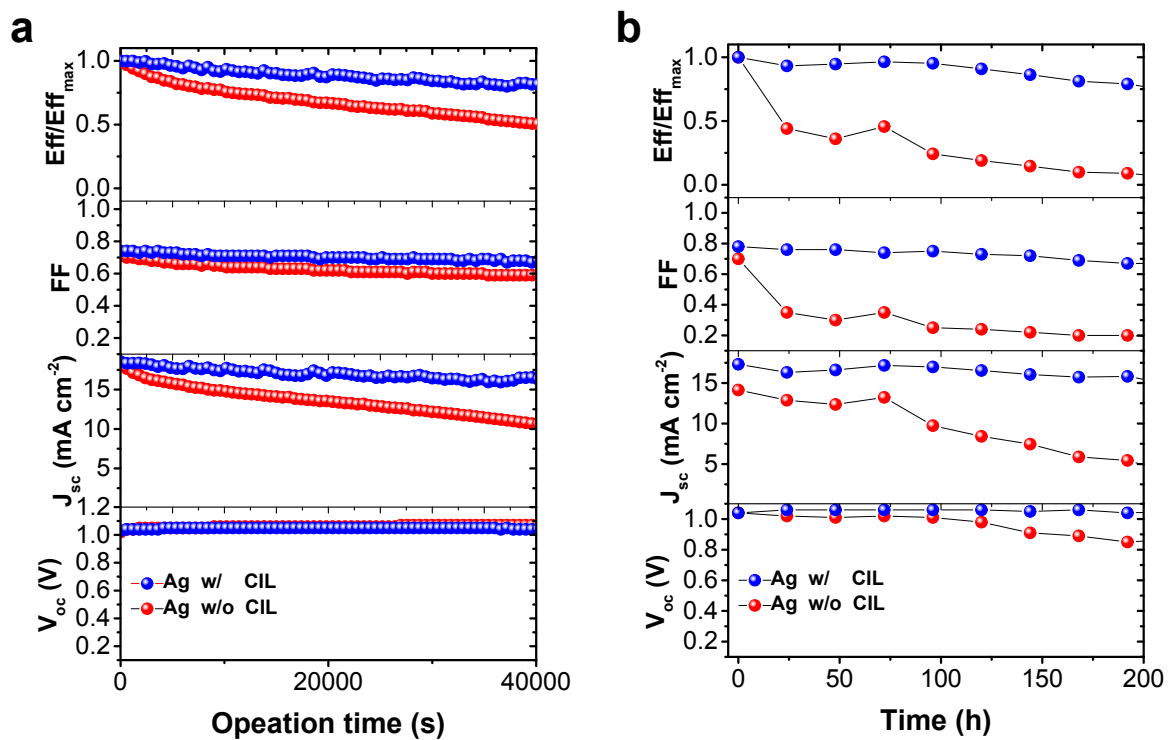


Figure S19. Device parameters during a, the illumination aging test under N₂ condition and b, dark storage under ambient condition.

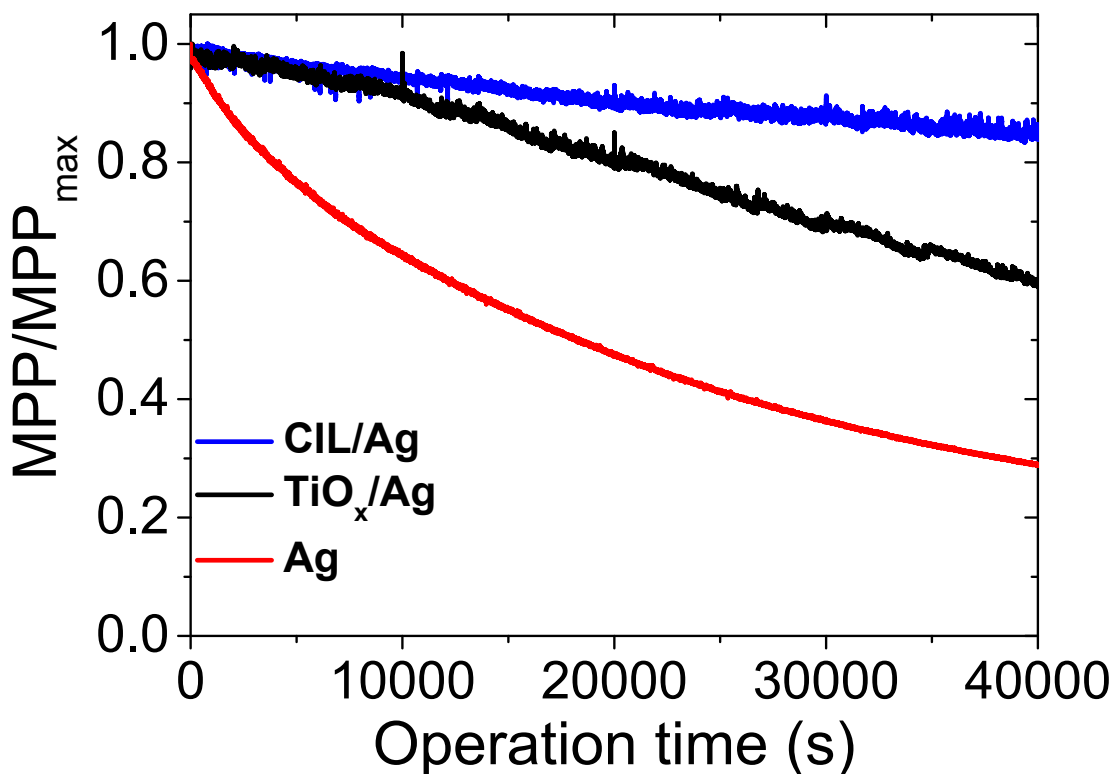


Figure S20. Normalized max power (tracked by max power point (MPP) method) of the PSC devices with bare Ag electrode, and with TiO_x/Ag and CIL/Ag configuration.

Note S7. We measured the operation stability of the PSC devices with the bare Ag electrode (as a reference device), TiO_x/Ag and CIL/Ag configuration using max power point (MPP) tracking method under the illumination of AM 1.5G, 100 mW cm⁻². As we expected, the reference devices showed the fastest degradation process of the device performance. Interestingly, the devices with the CIL exhibited the most stable devices performance among the devices. Despite the similar thickness and coverage of both TiO_x and CIL, the improved device stability can be attributed to the amine mediated metal oxide system of the CIL.

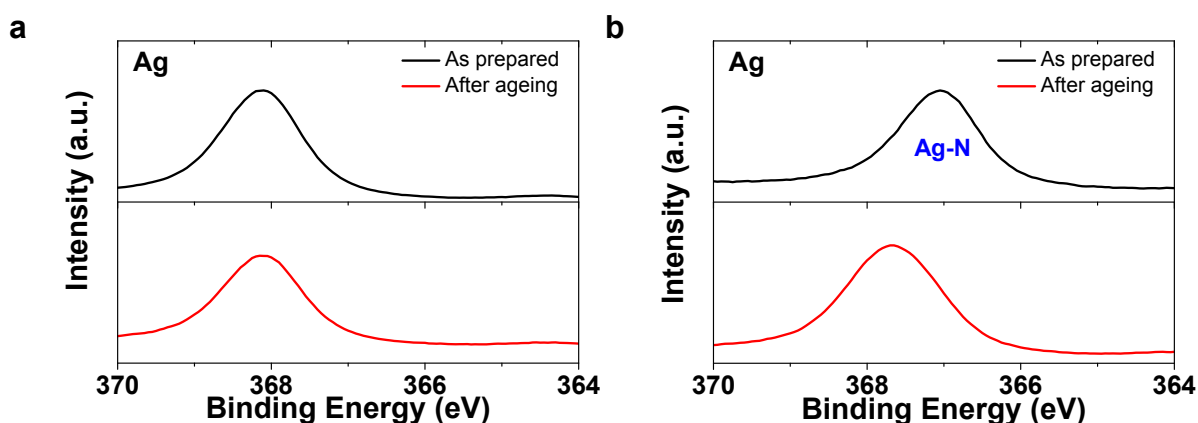


Figure S21. a,b, High-resolution XPS spectra of Ag on the ITO/PEDOT:PSS/ VO_x /perovskite/ PC_{60}BM /without and with CIL/Ag (5 nm) as a function of aging time. The Ag electrodes were deposited under a 5-nm-thick layer to measure the relationship of the interface between the Ag electrodes and under layers, such as the CIL and PC_{60}BM .

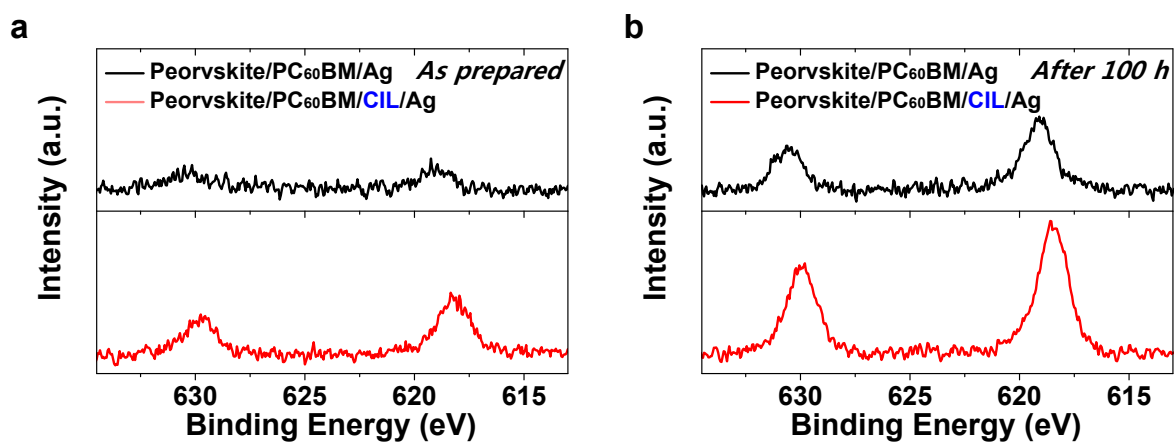


Figure S22. a,b, High-resolution XPS spectra for the iodine part of the pristine and aged samples, ITO/PEDOT:PSS/ VO_x /perovskite/ PC_{60}BM /without and with a CIL/Ag (5 nm). The sharper XPS signals of the sample containing the CIL indicate that more iodide ion defects were extracted from the perovskite layer than for the reference sample without the CIL.

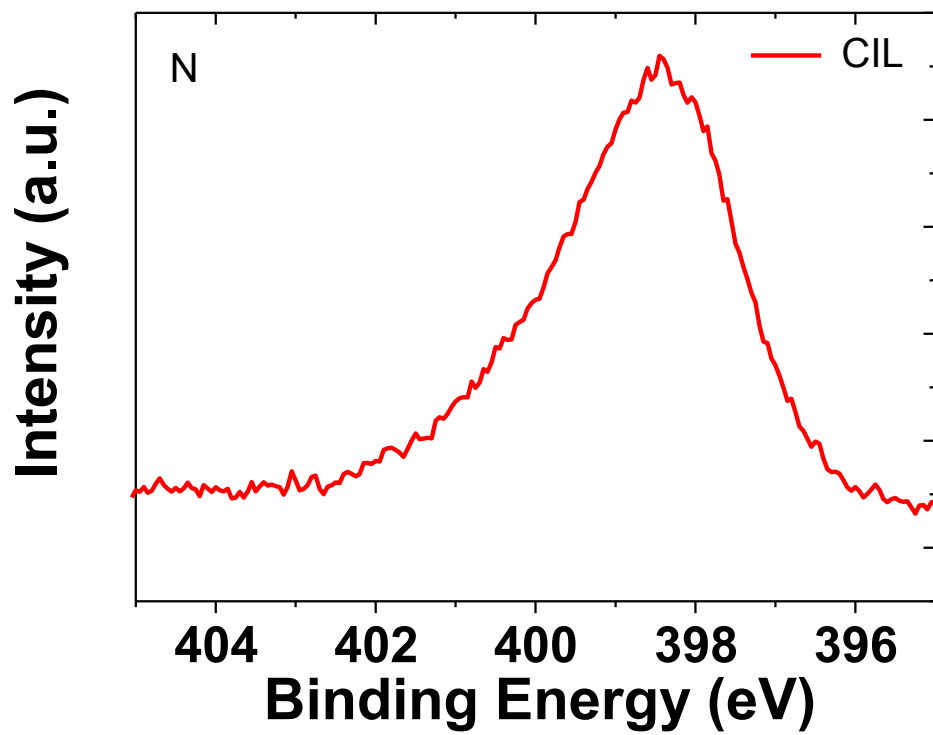


Figure S23. High resolution XPS spectra of N on the Si/CIL.

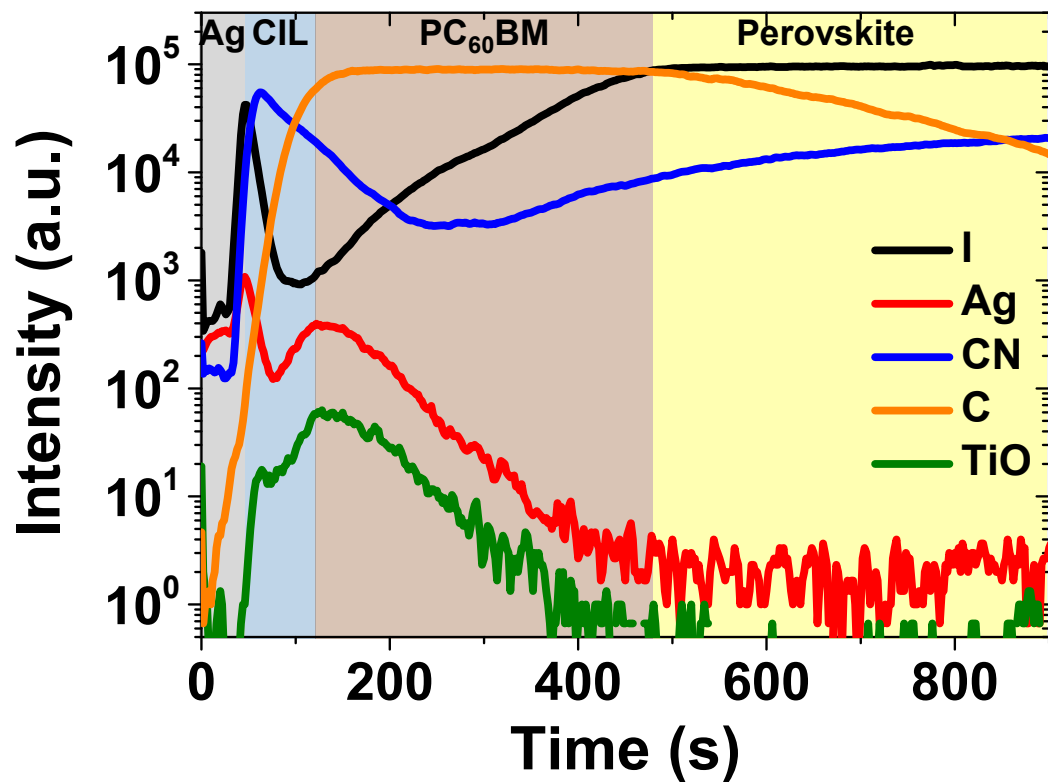


Figure S24. Depth profile of a p-i-n PSC with a CIL measured by time-of-flight secondary ion mass spectroscopy.

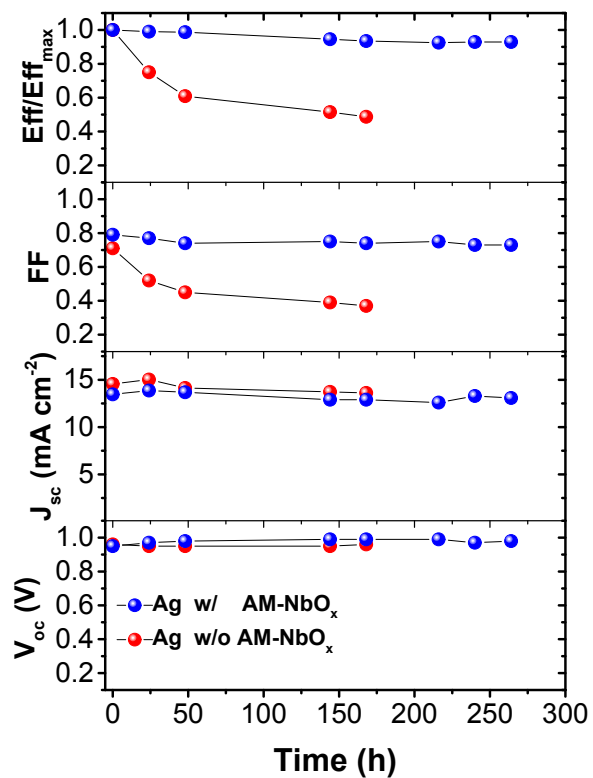


Figure S25. Lifetime test of p-i-n PSC devices with amine-mediated niobium suboxide (AM-NbO_x).

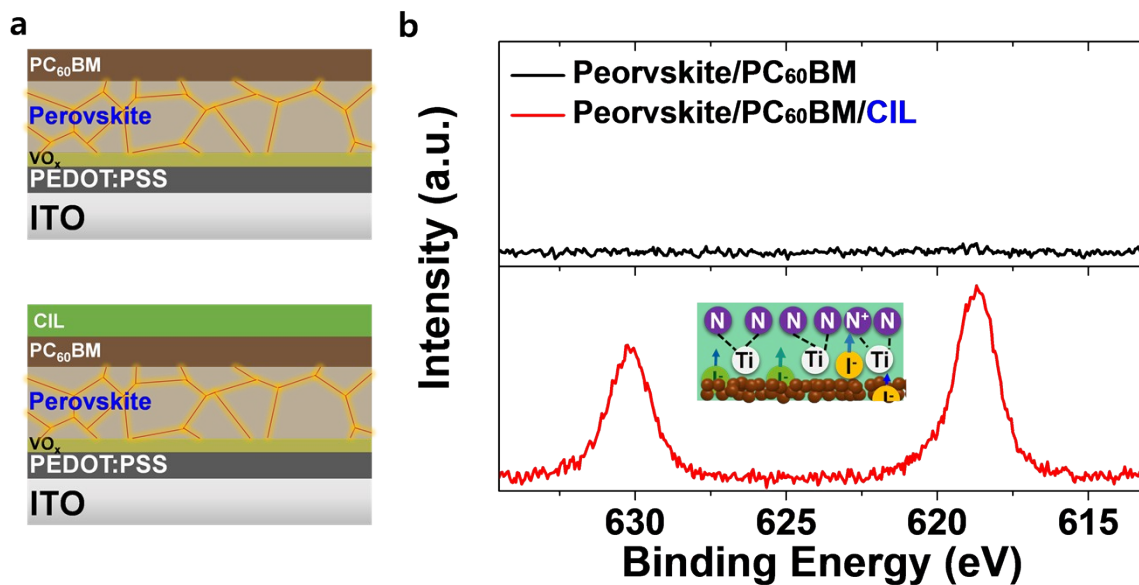


Figure S26. a,b, High resolution XPS spectra measured with a sample structure of ITO/PEDOT:PSS/VO_x/perovskite/PC₆₀BM/ without and with a CIL for the iodine part.

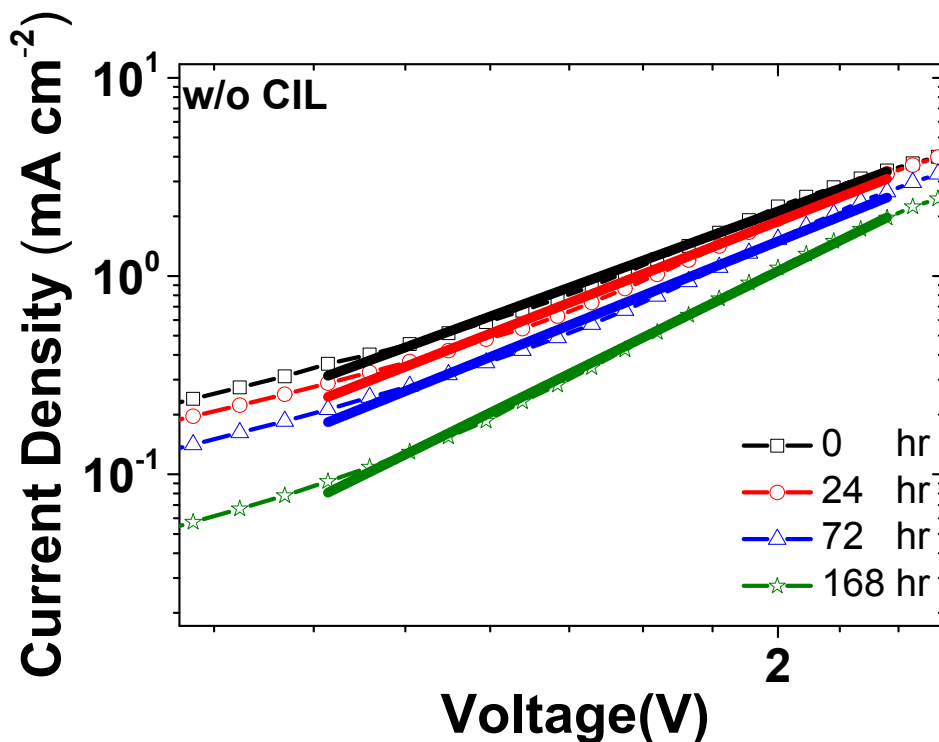


Figure S27. J - V characteristics of the electron-only device, ITO/C₆₀/perovskite/PC₆₀BM/with or without a CIL/Al.

Note S8. The characteristic energies (E_{ch}) were calculated from the J - V characteristics of the electron-only device (Figure S27)⁴.

$$E_{ch} = (l - 1)k_B T$$

, where l is the slope of the J - V characteristics ($l > 3$), k_B is Boltzmann constant, and T is temperature (300 K).

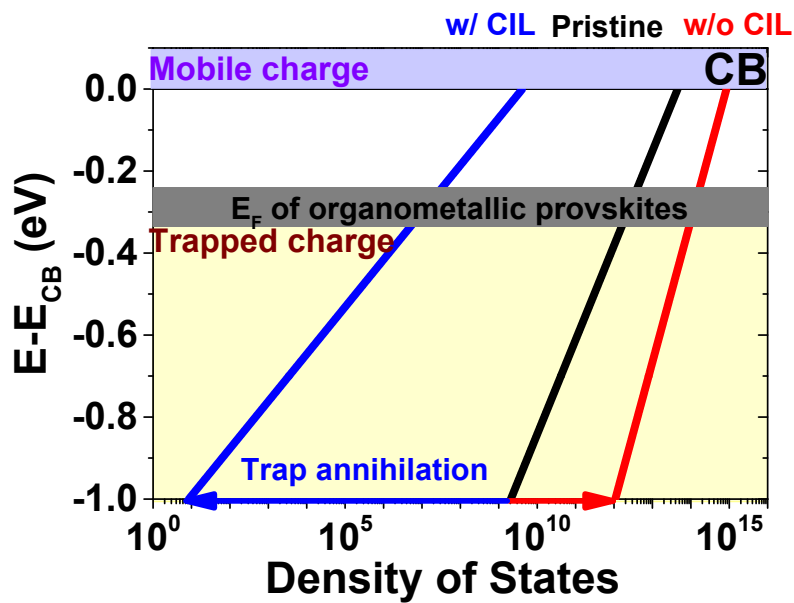


Figure S28. Distribution of trap states for the pristine and aged perovskite layer with/without a CIL.

Note S9. Since the trap-filled-limit voltages (V_{TFLS}) of all electron-only devices are same (~ 1.35 V as shown in Figure 3d and d), the total trap density (N_t) of the perovskite layers is also same (order of 10^{16} cm⁻³). The relation between the N_t and the onset voltage of V_{TFL}

regime is $N_t = \frac{2\varepsilon_r\varepsilon_0V_{TFL}}{ed^2}$, where ε_r represents the dielectric constant (25)⁵, ε_0 is the vacuum permittivity (8.85×10^{-14} F cm⁻¹), e is elementary charge (1.69×10^{-19} C), and d is thickness of the perovskite layers (300 nm). However, the smaller E_{ch} implies narrower deep-trap

distribution and it also represents the less trapped charge in localized states (Figure S28).

Assuming a trap distribution lying below the conduction band (CB) edge levels of the form:

$$N(E - E_{CB}) = \frac{N_t}{E_{ch}} e^{-\frac{E - E_{CB}}{E_{ch}}}$$

, where N_t is the total trap density, E_{ch} is the characteristic energy of the distribution and E_{CB} is the energy of the CB edge level. Because the Fermi levels of the organo-metallic perovskite materials generally locate 0.3-0.4 eV below the CB edge level⁶, reduced E_{ch} of the aged perovskite layer with a CIL represent less deep-trap charge as localized states below the Fermi level of the perovskite layer.

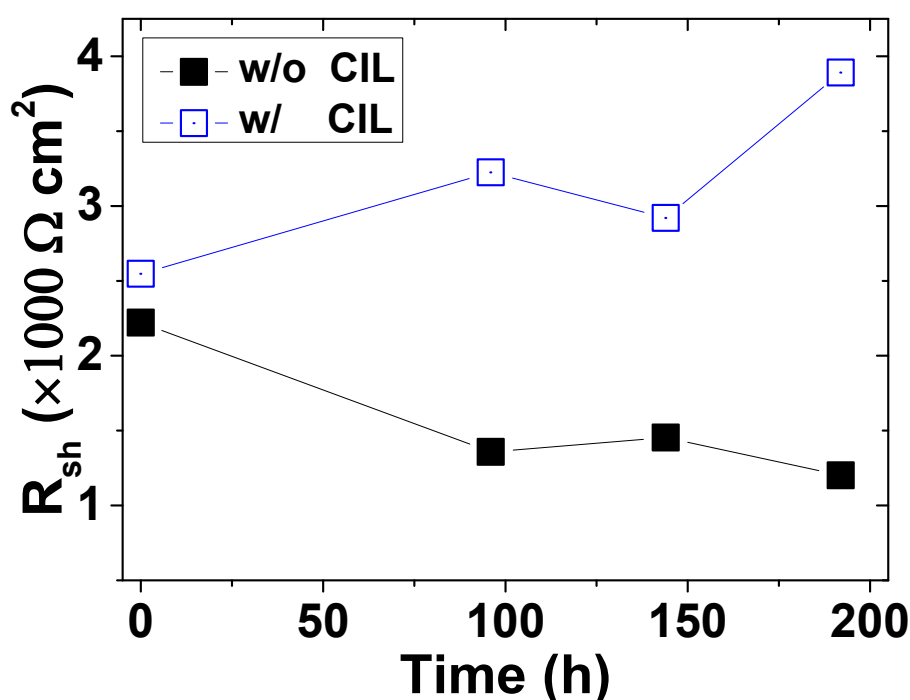


Figure S29. Shunt resistance (R_{sh}) of the Ag-electrode PSCs with and without the CIL.

Note S10. The Nyquist plot of the pristine reference device, under the open-circuit condition with illumination, exhibited one parallel resistance-capacitance (RC) element, which can be attributed to selective charge transport at the interface between the charge transport layers

and the perovskite layer in the high-frequency region ($> 10^4$ Hz), as shown in Figure 4a. After aging, the resistance for selective charge transport (R_{sc}) increased dramatically from 470 to $2,500 \Omega \text{ cm}^{-2}$, which is consistent with the large R_s of the reference PSC, as shown in Figure 1c. Interestingly, in the low-frequency region (< 10 Hz), the emergence of an additional inductive response can be interpreted as corrosion by the adsorbed halide ions at the Ag electrode⁷. In Figure 4b, the CIL device for both pristine and aged conditions showed two similar parallel RC elements combining with a small R_{sc} below $100 \Omega \text{ cm}^{-2}$ in the high-frequency region ($> 10^4$ Hz) and a chemical capacitance in the intermediate-frequency region ($\sim 10^3$ Hz) without the inductive response in the reference device. Based on the large single loop of the impedance for the TiO_x devices as shown in Figure S8b, the chemical capacitance of the CIL devices can be attributed to a response of the chemical interaction in the CIL, which implies that the CIL prevents the corrosion of the Ag electrode and maintains the small R_s of the device (see Figure 1f).

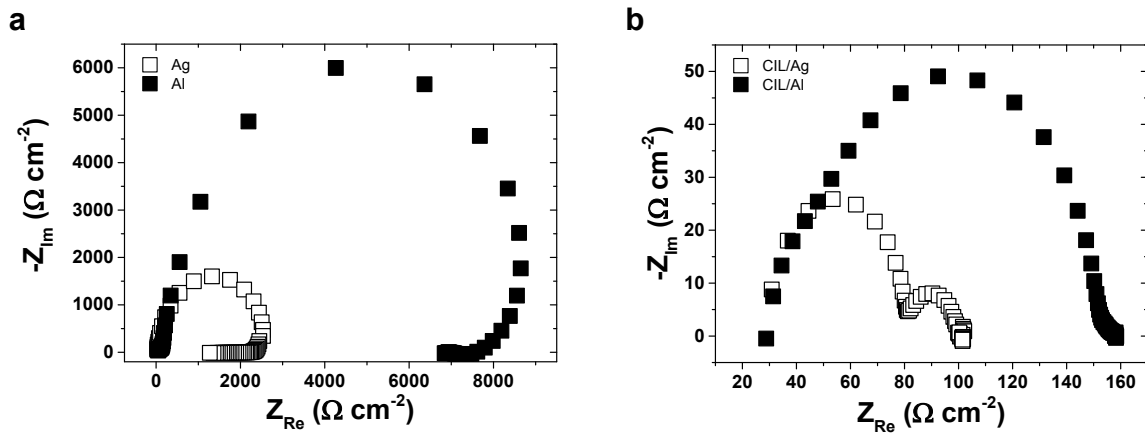


Figure S30. a,b, Impedance spectra measured at V_{oc} bias in under the AM 1.5G illumination conditions as the aged (200 h) Al- and Ag-electrode PSCs without and with the CIL.

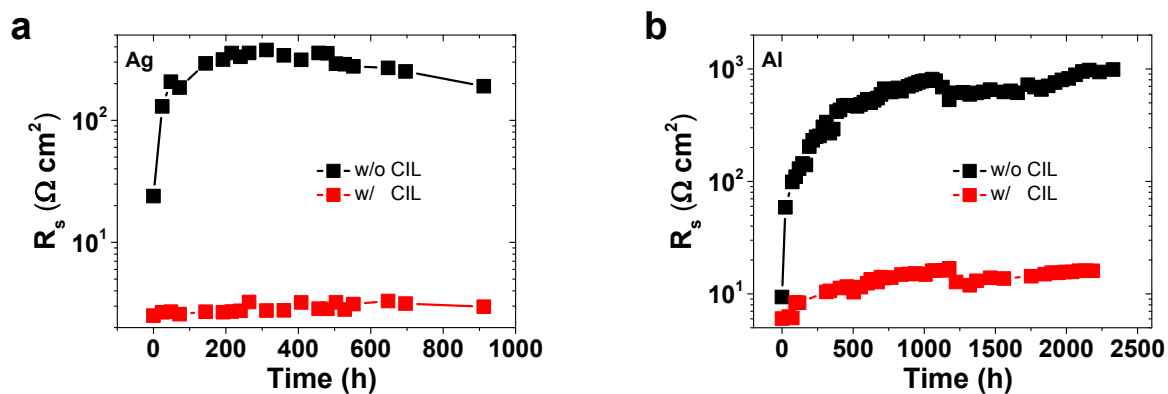


Figure S31. a,b, Series resistance (R_s) of the p-i-n PSC devices with Al and Ag electrodes, as a function of time.

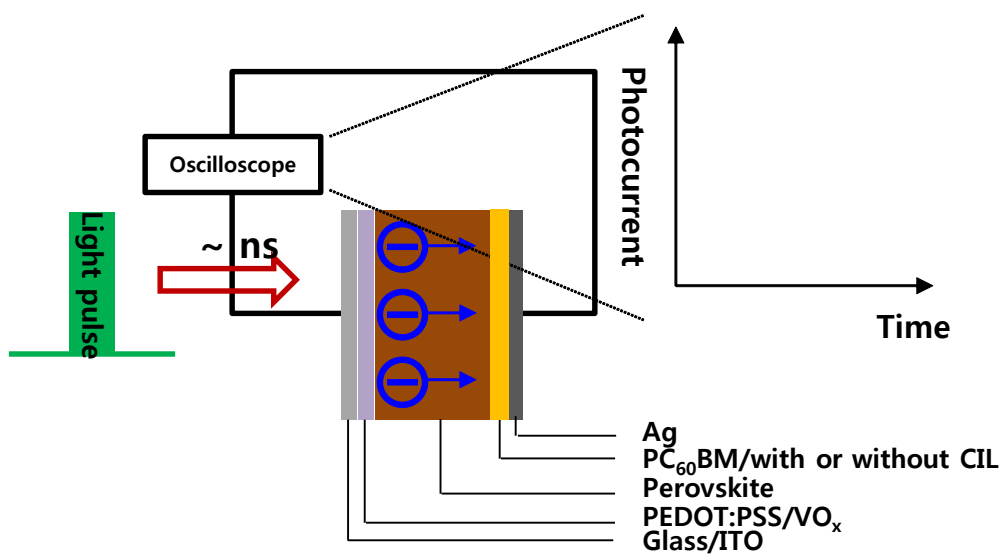


Figure S32. Schematic diagram of the transient photocurrent of the p-i-n PSC devices.

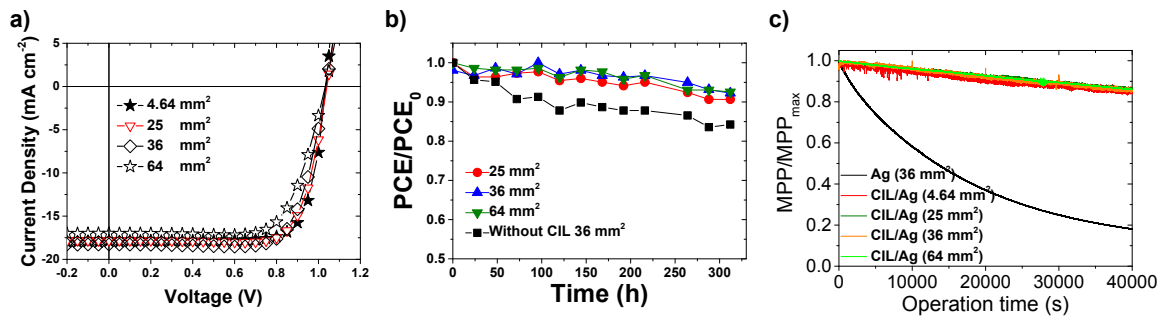


Figure S33. J - V , lifetime and steady-state photocurrent measurements. a, J - V curves for the optimized p-i-n PHJ perovskite solar cells with different sizes measured under AM 1.5G. b, c. The photovoltaic performances of the p-i-n PSCs and the steady-state photocurrent measurements, as functions of the storage time under N_2 .

Table S1. Summary of the J - V characteristics of the p-i-n PHJ PSCs (ITO/PEDOT:PSS /perovskite/PC₆₀BM/CIL/Ag) by varying device size.

Device area [mm ²]	V_{oc} [V]	J_{sc} [mA/cm ²]	FF	PCE [%]
4.64	1.03	17.88	0.77	14.31
25	1.04	17.81	0.77	14.18
36	1.04	18.28	0.75	14.10
64	1.03	16.99	0.71	12.54

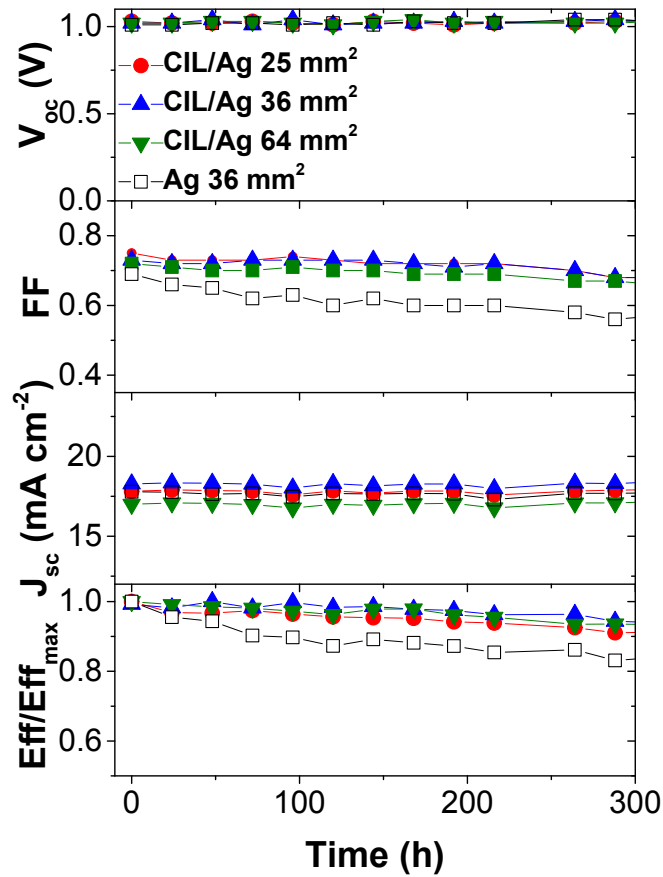


Figure S34. Device parameters of the large-area PSC devices during aging tests under N_2 condition.

References

- [1] N. J. Jeon, J. H. Noh, Y. C. Kim, W. S. Yang, S. Ryu and S. I. Seok, *Nat. Mater.*, 2014, 13, 897-903.
- [2] S. M. Sze and K. K. Ng, *Physics of Semiconductor Devices*, Wiley-interscience, 2006.
- [3] J. Kong, J. Lee, G. Kim, H. Kang, Y. Choi and K. Lee, *Phys. Chem. Chem. Phys.*, 2012, 14, 10547-10555.

- [4] M. M. Mandoc, B. de Boer, G. Paasch and P. W. M. Blom, *Phys. Rev. B*, 2007, 75, 193202.
- [5] A. Poglitsch and D. Weber, *J. Chem. Phys.*, 1987, 87, 6373-6378.
- [6] P. Schulz, E. Edri, S. Kirmayer, G. Hodes, D. Cahenb and A. Kahn, *Energy Environ. Sci.*, 2014, 7, 1377-1381.
- [7] R. S. Sanchez, V. Gonzalez-Pedro, J.-W. Lee, N.-G. Park, Y. S. Kang, I. Mora-Sero and J. Bisquert, *J. Phys. Chem. Lett.*, 2014, 5, 2357-2363.